Loss-of-function mutation in *Hippo* suppressed enlargement of lysosomes and neurodegeneration caused by *dFIG4* knockdown

Yukie Kushimura[a], Yumiko Azuma[a], Ikuko Mizuta[a], Yuuka Muraoka[c,d], Akane Kyotani[c,d], Hideki Yoshida[c,d], Takahiko Tokuda[a,b], Toshiki Mizuno[a] and Masamitsu Yamaguchi[c,d]

Charcot–Marie–Tooth disease (CMT) is the most common hereditary neuropathy, and more than 80 CMT-causing genes have been identified to date. CMT4J is caused by a loss-of-function mutation in the *Factor-Induced-Gene 4* (*FIG4*) gene, the product of which plays important roles in endosome–lysosome homeostasis. We hypothesized that *Mammalian sterile 20-like kinase* (*MST*) *1* and *2*, tumor-suppressor genes, are candidate modifiers of CMT4J. We therefore examined the interaction between *dFIG4* and *Hippo* (*hpo*), *Drosophila* counterparts of FIG4 and MSTs, respectively, using the *Drosophila* CMT4J model with the knockdown of *dFIG4*. The loss-of-function allele of *hpo* improved the rough eye morphology, locomotive dysfunction accompanied by structural defects in the presynaptic terminals of motoneurons, and the enlargement of lysosomes caused by the knockdown of *dFIG4*. Therefore, we identified *hpo* as a modifier of phenotypes induced by the knockdown of *dFIG4*. These results in *Drosophila* may provide an insight into the pathogenesis of CMT4J and contribute toward the development of disease-modifying therapy for CMT. We also identified the regulation of endosome–lysosome homeostasis as a novel probable function of Hippo/MST. *NeuroReport* 29:856–862

NeuroReport 2018, **29**:856–862

Keywords: CMT, CMT4J, *Drosophila*, endosome–lysosome system, FIG4, Hippo pathway, Hippo, lysosome, MST1, neurodegeneration

[a]Department of Neurology, [b]Department of Molecular Pathobiology of Brain Diseases, Kyoto Prefectural University of Medicine, [c]Department of Applied Biology and [d]The Center for Advanced Insect Research, Kyoto Institute of Technology, Kyoto, Japan

Correspondence to Masamitsu Yamaguchi, PhD, Department of Applied Biology, Kyoto Institute of Technology, Matsugasaki, Sakyo-ku, Kyoto 606-8585, Japan
Tel: +81 52 724 7781; fax: +81 52 724 7799; e-mail: myamaguc@kit.ac.jp

Received 2 April 2018 **accepted** 16 April 2018

Introduction

Charcot–Marie–Tooth disease (CMT) is the most common hereditary neuropathy characterized by progressive motor and sensory polyneuropathies. CMT may be inherited in an autosomal dominant, an autosomal recessive, or an X-linked manner and more than 80 CMT-causing genes have been identified to date [1]. CMT4J (OMIM #611228) is a severe, autosomal recessive inherited CMT caused by loss-of-function mutations in the *Factor-Induced-Gene 4* (*FIG4*) gene [2]. There is currently no specific treatment for CMT4J.

The endosome–lysosome system and autophagy are considered to play important roles in the pathogenesis of neurodegenerative diseases [3,4]. FIG4 has been suggested to be crucially involved in endosome–lysosome membrane homeostasis because loss-of-function mutations in *FIG4* counterparts induced enlarged vacuoles or lysosomes in yeast [5,6], nematodes [6], and mice [2]. As endosomes and lysosomes are required for autophagy, the loss of *FIG4* is expected to cause impaired autophagy, which is supported by previous findings obtained from *FIG4* null mice [7]. These findings indicated that molecules related to endosome–lysosome membrane homeostasis and/or autophagy modify the function of *FIG4*. The endosome–lysosome homeostasis is a potential target in the treatment of CMT4J; however, limited information is currently available.

Genetic interaction assays using *Drosophila* are a strong tool for identifying genetic modifiers for disease-related genes. We reported previously that the knockdown of *Drosophila FIG4* (*dFIG4*) induced an aberrant eye morphology, shortened branches of motoneurons, and mobility defects in the *Drosophila* CMT4J model [8]. We also observed the enlargement of lysosomes in *dFIG4* knockdown *Drosophila* [8], which was consistent with another group's findings using the null mutation of *dFIG4* [9].

In the present study, as an initial step to identify modifier genes for the *dFIG4* knockdown phenotype, we focused on the cancer-related gene *Hippo* (*hpo*). Some causative genes of familial amyotrophic lateral sclerosis (ALS), which is characterized by the progressive loss of motoneurons, appear to be involved in cancer [10]. This finding suggests that cancer-related genes modify the neurodegeneration process. The tumor-suppressor gene, *Hippo*, which is the *Drosophila* ortholog of *Mammalian sterile 20-like kinase (MST) 1 and 2*, encodes one of the core

 DOI: 10.1097/WNR.0000000000001044

proteins of the Hippo pathway [11]. A hyperactivated Hippo pathway has been observed in neurodegenerative diseases, including Alzheimer's disease and ALS [12]. Although the relationship between *hpo* and endosome–lysosome homeostasis currently remains unknown, *hpo* has been reported to regulate autophagy [13–16]. On the basis of these findings, we hypothesized that *hpo* could be a candidate modifier of *FIG4*.

To test our hypothesis that *hpo* is a modifier of *FIG4*, we analyzed the interaction between the knockdown of *dFIG4* and the loss-of-function allele of *hpo* using a *Drosophila* model.

Materials and methods

Fly stocks

Fly stocks were maintained at 25°C on standard food containing 0.65% agar, 10% glucose, 4% dry yeast, 5% corn flour, and 3% rice bran. The following fly strains were obtained from the Bloomington *Drosophila* Stock Center (BDSC): w; $P[w^{+mC} = GAL4\text{-}elav.L]^{3}$ (BDSC 8760)(elav-GAL4), $P[ry^{+t7.2} = hsFLP]^{12}$, $y^{1}w^{*};P[ry^{+t7.2} = neoFRT]^{42}$ $Dhpo^{KS240}/CyO$ (BDSC 25085)(hpo^{KS240}), $y^{d2}w^{1118}P[ry^{+t7.2} = ey\text{-}FLP.N]^{2};P[ry^{+t7.2} = neoFRT]^{42}Dhpo^{KC202}/CyO$, $P[w^{+mC} = GAL4\text{-}Kr.C]^{DC3}$, $P[w^{+mC} = UAS\text{-}GFP.S65T]^{DC7}$ (BDSC 25090)(hpo^{KC202}), and w^{1118}; *and* $P[w^{+mC} = UAS\text{-}GFP.dsRNA.R]^{143}$ (BDSC 9331)(UAS-GFP-IR). $y^{1}w^{1118}$. $P[w^{+mC} = Lsp2\text{-}GAL4.H]^{3}$ (BDSC 108752)(FB-GAL4) was obtained from the Kyoto Stock Center. The RNAi line targeting the region corresponding to amino acid residues 605–714 of dFIG4 (UAS-dFIG4-IR$_{605–714}$) was obtained from the Vienna *Drosophila* Resource Center. The establishment of the lines carrying GMR-GAL4 has been described previously [17]. Fly lines bearing UAS-dFIG4-IR have been described previously [8]. The phenotypes of these lines were not because of a possible insertional mutation or off-target effect as described previously [8].

Scanning electron microscopy

For compound eye observations, adult flies were anesthetized with diethyl ether, mounted on stages, and inspected under the scanning electron microscope V-7800 (Keyence Inc., Osaka, Japan) [18]. In each experiment, at least six adult flies were selected randomly from each line for scanning electron microscopy to inspect eye morphologies. In each experiment, no significant variations were observed in eye phenotypes among six individuals from the same strain.

Immunohistochemistry

In the visualization of neuromuscular junctions (NMJs), third instar larvae were dissected in HL3 saline [19] and then fixed in 4% paraformaldehyde/PBS for 30 min. The blocking solution contained 2% bovine serum albumin and 0.1% Triton X-100 in PBS. FITC-conjugated goat anti-horseradish peroxidase (HRP) (1 : 1000; MP Biochemicals, Tokyo, Japan) was used as the detection antibody. Samples were mounted in Vectashield (Vector Laboratories; Burlingame, California, USA) and inspected under a confocal laser scanning microscope (Olympus FluoView FV10i; Olympus, Tokyo, Japan). Motoneurons in muscle 4 in abdominal segment 2 were inspected. The Meta Morph Imaging System 7.7 (Molecular Devices Inc., San Jose, California, USA) was used to measure nerve terminal branch lengths and Ib bouton sizes.

In the visualization of lysosomes, fat bodies were collected by dissecting third instar larvae in PBS and stained with 100 nM of LysoTracker Blue DND22 (Invitrogen, Tokyo, Japan) for 1 min. Stained samples were washed twice with PBS, mounted in Vectashield (Vector Laboratories, Burlingame, California, USA), and observed under a confocal laser scanning microscope (Olympus FluoView FV10iOlympus, Tokyo, Japan). The Meta Morph Imaging System 7.7 (Molecular Devices Inc.San Jose, California, USA) was used to measure the diameters of lysosomes.

Crawling assay

Crawling assays were performed as described previously [20]. Third instar male larvae were placed in a 14-cm Petri dish containing 2% agarose (previously poured and allowed to harden) over a black sheet at a density of five larvae per dish. Larvae moved for 30 s, a video was recorded for 1 min, and the path of each larva and its moving speed were analyzed using ImageJ (Image Processing and Analysis in Java) (NIH; Bethesda, Maryland, USA).

Data analysis

Graph Pad Prism version 6.0 (MDF, Tokyo, Japan) was used to carry out each statistical analysis. A one-way analysis of variance was used to assess the significance of comparisons between groups of data. When the one-way analysis of variance showed a significant variation among groups, Dunnett's test was used for pairwise comparisons between groups. All data are shown as the mean ± standard error.

Results

The loss-of-function mutation in *hpo* significantly suppressed the rough eye morphology caused by the eye-specific *dFIG4* knockdown

Flies with the eye disc-specific *dFIG4* knockdown showed the rough eye morphology in adults, as we reported previously (Fig. 1a) [8]. Two loss-of-function alleles among *hpo*, hpo^{KS240}, and hpo^{KC202} in the heterozygous state markedly attenuated the aberrant compound eye morphology induced by the eye disc-specific *dFIG4* knockdown (GMR > UAS-dFIG4-IR/hpo^{KS240} and GMR > UAS-dFIG4-IR/hpo^{KC202}) (Fig. 1b and c). The suppressive effect observed was not because of potential background mutations because two independent loss-of-function alleles of *hpo* showed similar suppressive effects. These results indicate that *dFIG4* genetically interacts with *hpo*.

Fig. 1

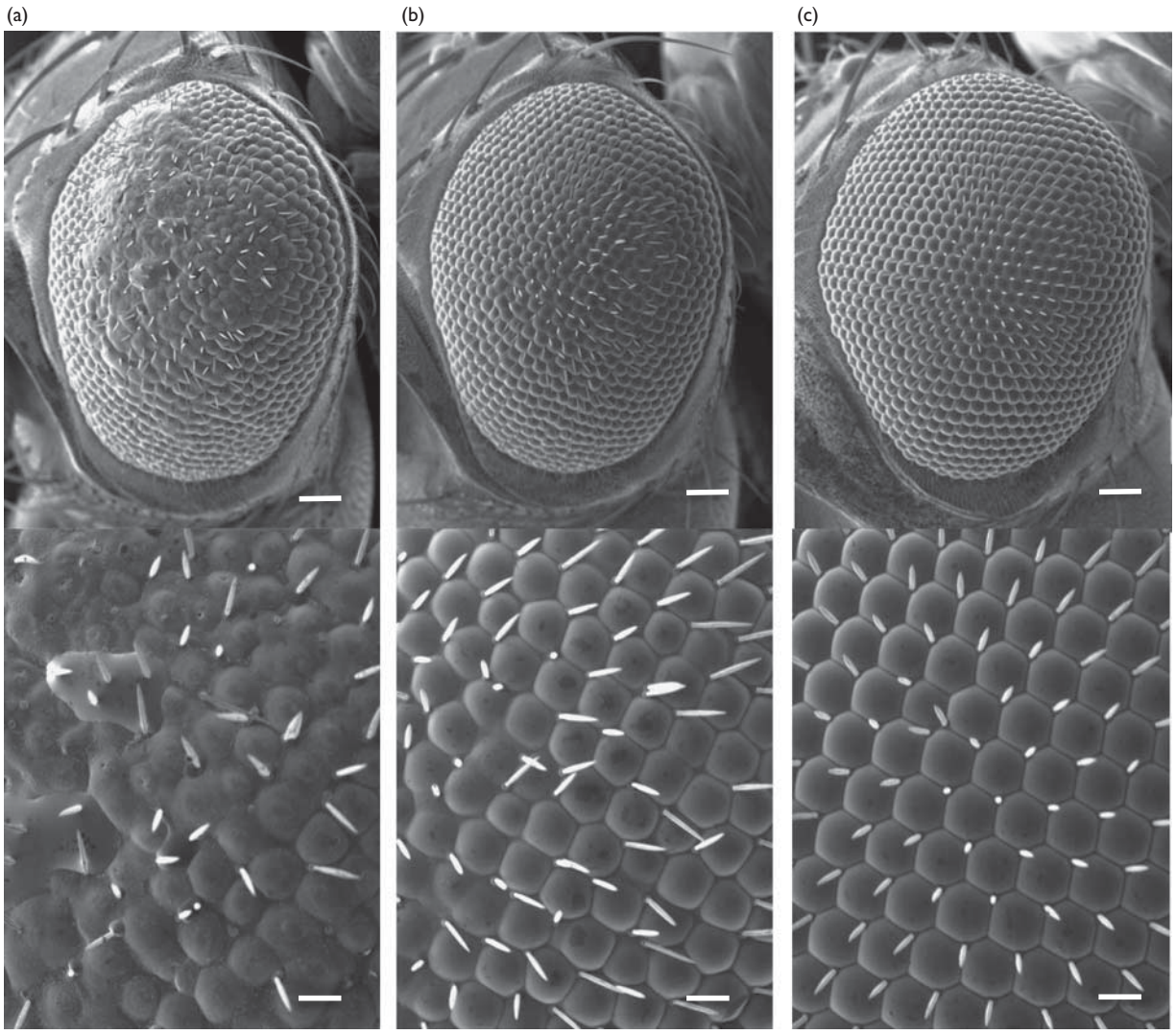

The rough eye morphology induced by the *dFIG4* knockdown is suppressed by the loss-of-function mutation in *hpo*. Each panel shows a scanning electron micrograph of the adult compound eye. Each lower panel shows a higher magnification image of the corresponding upper panel. (a) *GMR-GAL4/Y*; *UAS-dFIG4-IR/+*; + (GMR > UAS-dFIG4-IR). (b) *GMR-GAL4/Y; UAS-dFIG4-IR/hpo^{KC202};* + (GMR > UAS-dFIG4-IR/hpo^{KC202}). (c) *GMR-GAL4/Y; UAS-dFIG4-IR/hpo^{KS240}*; + (GMR > UAS-dFIG4-IR/hpo^{KS240}). Posterior is to the right and dorsal is to the top. Flies were developed at 28°C. Scale bars in each upper panel indicate 50 μm and scale bars in the bottom panel indicate 14.2 μm.

The loss-of-function mutation in *hpo* suppressed shortened motoneurons at presynaptic terminals in the NMJ caused by the *dFIG4* knockdown

We analyzed the effects of the loss-of-function allele of *hpo* on the aberrant morphology of larval motoneuron terminals induced by the neuron-specific *dFIG4* knockdown. Neuron-specific *dFIG4* knockdown resulted in shorter presynaptic terminal branches of motoneurons in the NMJ (Fig. 2c) than those in the control (Fig. 2a), as reported previously [8]. The total branch length of the motoneuron at the NMJ was significantly longer in larvae carrying the *dFIG4* knockdown with the loss-of-function mutation in *hpo* (elav > UAS-dFIG4-IR/hpo^{KS240}, Fig. 2d and e, black column) than in larvae carrying the dFIG4 knockdown only (elav > UAS-dFIG4-IR, Fig. 2c and e, gray column) (67.60 ± 5.97 vs. 81.44 ± 3.84 μm, $P < 0.05$, Fig. 2e). The total branch length of the motoneuron at the NMJ of larvae carrying the loss-of-function mutation in *hpo* only (hpo^{KS240}/+, Fig. 2b and e, hatched column) was similar to that of control larvae (elav > UAS-GFP-IR, Fig. 2a and e, white column) (121.62 ± 13.19 vs. 115.35 ± 9.49 μm, $P = 0.12$, Fig. 2e). Thus, a half-dose reduction in *hpo* suppressed the morphological changes in presynaptic terminals induced by the neuron-specific *dFIG4*

Fig. 2

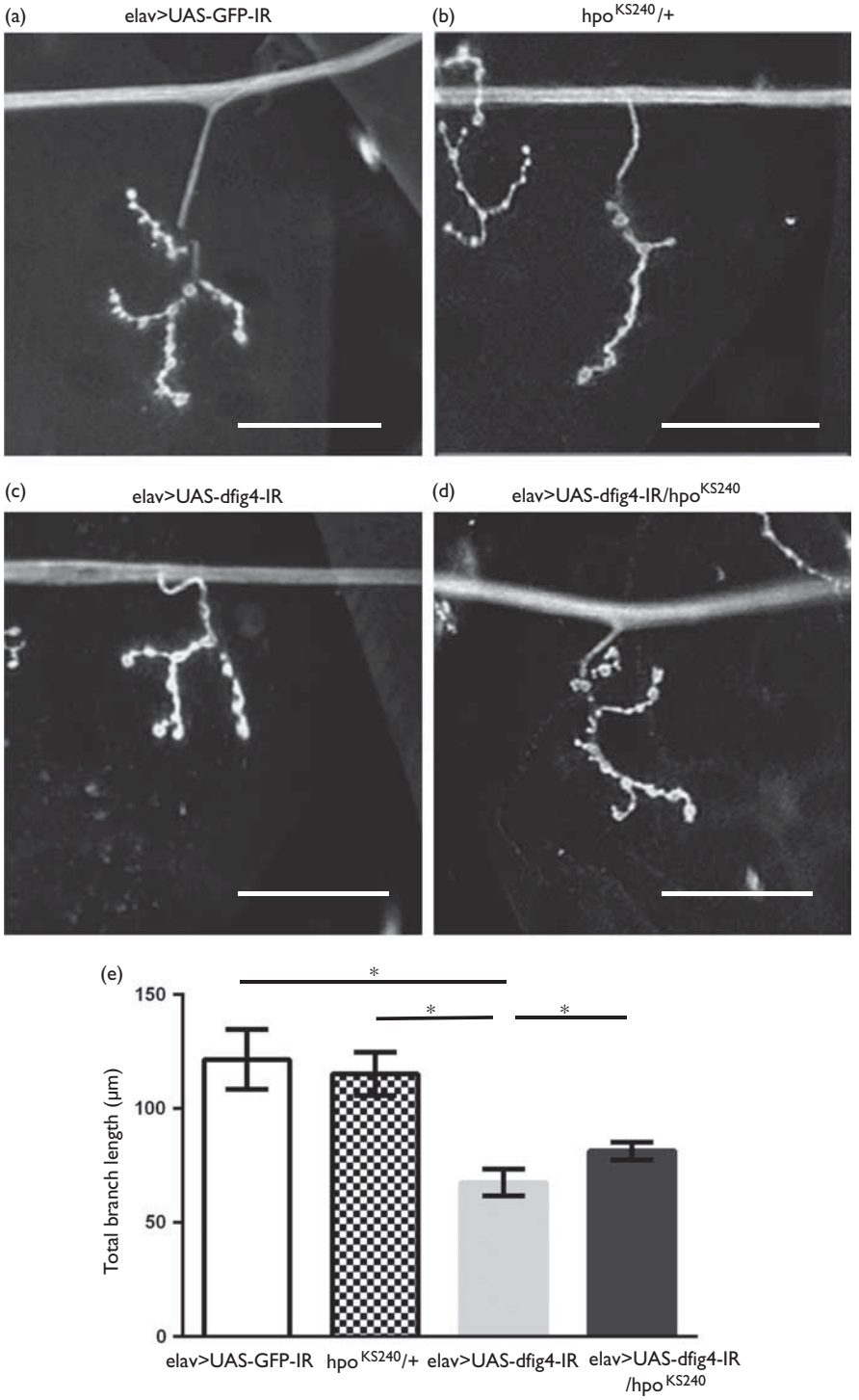

Shortened motoneurons in the neuromuscular junction caused by the *dFIG4* knockdown are improved by the loss-of-function mutation in *hpo*. Each panel shows a representative image of anti-HRP staining of muscle 4 synapses in third instar larvae. (a) *yw/Y; UAS-GFP-IR/+; elav-GAL4/+* (elav > UAS-GFP-IR, control), (b) *yw/Y;hpo^{KS240}/+; +* (hpo^{KS240}/+), (c) *yw/Y; UAS-dFIG4-IR/+; elav-GAL4/+* (elav > UAS-dFIG4-IR), (d) *yw/Y; UAS-dFIG4-IR/hpo^{KS240}; elav-GAL4/+* (elav > UAS-dFIG4-IR/hpo^{KS240}). (e) The quantified total branch length of the motoneuron at the NMJ. Columns and horizontal bars show the mean and SE of measurements, respectively. *$P < 0.05$. The scale bars indicate 50 μm.

knockdown. As *elav*-GAL4 is a pan neuron-specific driver, further analysis with a motor neuron-specific GAL4 driver would be necessary to further confirm these results.

The loss-of-function mutation in *hpo* suppressed the reduced crawling ability induced by the *dFIG4* knockdown

To examine the locomotive ability of larvae carrying the neuron-specific *dFIG4* knockdown, we performed the well-established crawling assay [20]. Larvae carrying the *dFIG4* knockdown (elav > UAS-dFIG4-IR, Fig. 3, gray columns, $n = 21$) showed significantly shorter crawling distances within 30 s and also slower average crawling speeds than control larvae (elav > UAS-GFP-IR, Fig. 3, white columns, $n = 28$) (9.04 ± 1.36 vs. 16.38 ± 1.09 mm, $P < 0.001$, Fig. 3a) (0.58 ± 0.05 vs. 0.74 ± 0.03 mm/s, Fig. 3b). Larvae carrying the *dFIG4* knockdown with the loss-of-function mutation in *hpo* (elav > UAS-dFIG4-IR/hpo^{KS240}, Fig. 3, black columns, $n = 20$) showed significantly longer crawling distances (9.04 ± 1.36 vs. 18.76 ± 1.43 mm, $P < 0.001$, Fig. 3a) (0.58 ± 0.05 vs. 0.81 ± 0.04 mm/s, $P < 0.001$, Fig. 3b). Larvae carrying the loss-of-function mutation in *hpo* only (hpo^{KS240}/+, Fig. 3, hatched columns, $n = 22$) showed similar crawling ability to control larvae (17.50 ± 1.51 vs. 16.38 ± 1.09 mm, $P = 0.68$, Fig. 3a) (0.79 ± 0.05 vs. 0.74 ± 0.03 mm/s, $P = 0.50$, Fig. 3b). Thus, the half-dose reduction in *hpo* effectively suppressed the locomotive defect induced by the neuron-specific *dFIG4* knockdown.

Fig. 3

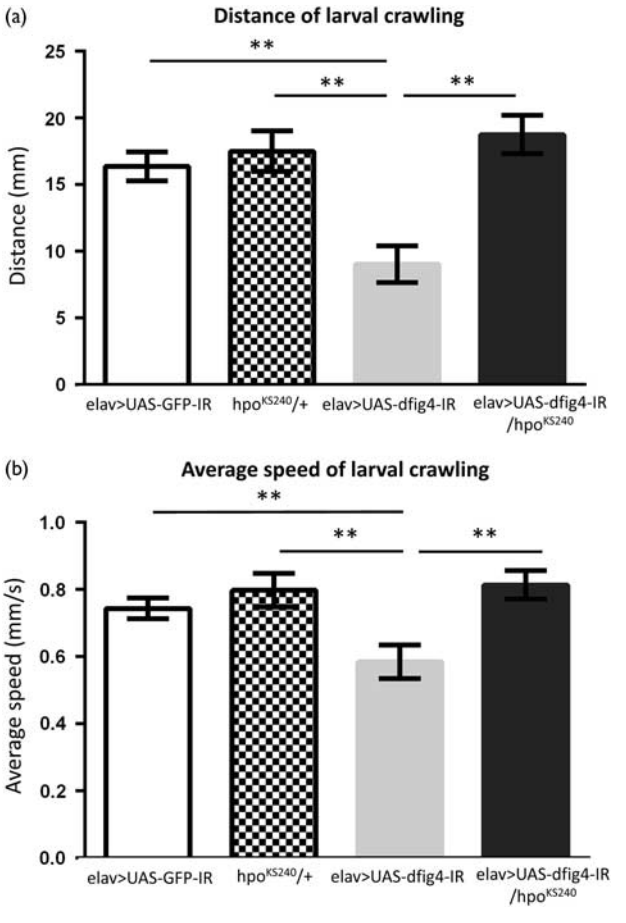

Reduced crawling ability induced by the *dFIG4* knockdown is suppressed by the loss-of-function mutation in *hpo*. (a) Average larval crawling distance (mm) within 30 s. (b) Average crawling speed (mm/s). Columns and horizontal bars show the mean and SE of measurements, respectively. $^{**}P < 0.001$.

The loss-of-function mutation in *hpo* suppressed the enlarged lysosome diameter induced by the *dFIG4* knockdown

As we reported previously, the *dFIG4* knockdown induced the enlargement of lysosomes in *Drosophila* in the larval fat body (Fig. 4) [8]. Larvae carrying the *dFIG4* knockdown (FB > UAS-dFIG4-IR, Fig. 4b and d, light gray column, $n = 18$) had lysosomes with significantly wider diameters than control larvae (FB > UAS-GFP-IR, Fig. 4a and d, white column, $n = 18$) (2.77 ± 0.57 vs. 6.43 ± 1.93 mm, $P < 0.001$, Fig. 4d). Larvae carrying the fat body-specific *dFIG4* knockdown with the loss-of-function mutation in *hpo* (FB > UAS-dFIG4-IR/hpo^{KS240}, Fig. 4c and d, gray column, $n = 18$) showed significant suppression of the enlarged diameters of lysosomes (6.43 ± 1.93 vs. 3.59 ± 0.92 mm, $P < 0.001$, Fig. 4d). Thus, the half-dose reduction in *hpo* effectively suppressed the abnormal enlargement of lysosomes induced by the fat body-specific *dFIG4* knockdown.

Discussion

A previous study reported that Hippo/MST is a genetic modifier of neurodegeneration in some ALS models. In *superoxide dismutase 1* (*sod1*) mouse ALS models, the downregulation of MST delays the onset of disease and extends survival [13]. Furthermore, reductions in the *hpo* gene dose suppress the eye degeneration phenotype and climbing defect in ALS *Drosophila* models targeted to *VAPB* [21]. However, a relationship between CMT and Hippo/MST has not yet been reported. In addition to the suppressive effect of the rough eye phenotype by the *dFIG4* knockdown, we found that the mutation in *hpo* effectively attenuated the reduced locomotive ability and abnormal formation of motoneurons induced by the neuron-specific *dFIG4* knockdown. Therefore, the present study is the first to indicate a relationship between CMT and *hpo* in a *Drosophila* model. Furthermore, Hippo/MST has potential as a candidate therapeutic target for CMT4J. The present study also uncovered a novel probable function of *hpo*, namely, the downregulation of endosome–lysosome homeostasis, as suggested by the result that the *dFIG4* knockdown-induced enlargement of lysosomes was ameliorated by the loss-of-function allele of *hpo*.

Fig. 4

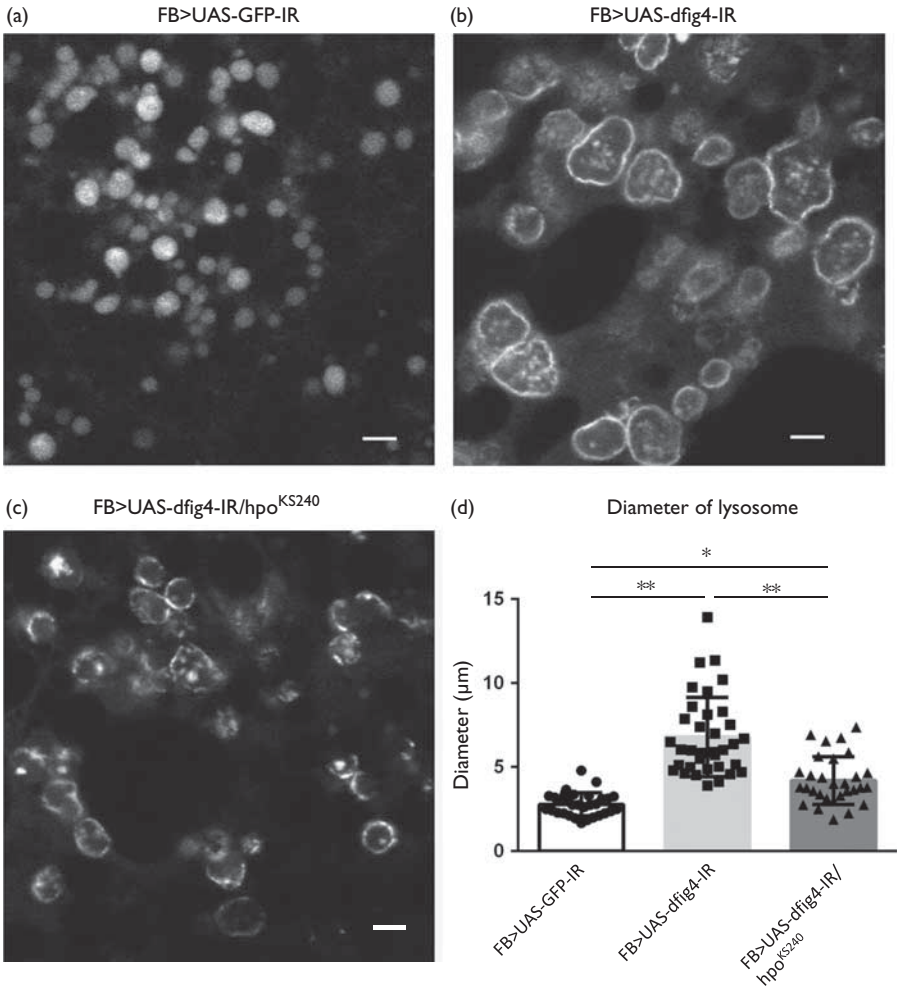

Enlarged lysosomes induced by the *dFIG4* knockdown are recovered by the loss-of-function mutation in *hpo*. Larval fat bodies were stained with LysoTracker to visualize lysosomes. (a) *yw/Y*; *UAS-GFP-IR/+*; *FB-GAL4/+* (FB > UAS-GFP-IR). (b) *yw/Y*; *UAS-dFIG4-IR/+*; *FB-GAL4/+* (FB > UAS-dFIG4-IR). (c) *yw/Y;UAS-dFIG4-IR/hpo^{KS240}*; *FB-GAL4/+* (FB > UAS-dFIG4-IR/hpo^{KS240}). (d) This graph shows the average diameter (μm) of lysosomes in larval fat bodies. The scale bars indicate 5 μm. *$P < 0.05$, **$P < 0.001$.

Limited information is currently available on the molecular mechanisms by which *hpo* influences *dFIG4* knockdown-related phenotypes. FIG4 interacts with FAB1 kinase and the scaffolding protein VAC14. The FIG4-VAC14-FAB1 complex functions to increase the abundance of PI(3,5)P_2, a signaling lipid located on the cytosolic surface of membranes of the late endosomal compartment [22]. To date, there have been no studies on protein–protein interactions between Hippo and a certain component of the FIG4-VAC14-FAB complex, or on the influence of the Hippo pathway on the abundance of PI(3,5)P_2. Therefore, further intensive studies are needed to clarify how Hippo regulates endosome–lysosome homeostasis.

The effects of the Hippo pathway on the regulation of autophagy remain controversial. Previous studies reported the upregulation of autophagy by Hippo, whereas others reported downregulation [13–16]. Our results support the Hippo pathway downregulating autophagy. This is consistent with previous findings showing that *MST1*, the mammalian homologue of *Hippo*, mediated abnormal autophagy in the *SOD1* ALS model mouse [13] and that an *MST1* deficiency enhanced autophagy in post-traumatic spinal motoneurons [14]. However, autophagy was shown to be upregulated by the Hippo pathway in a cell culture study or *Drosophila* model of Dantato-rubro-pallidoluysian atrophy [15,16]. These controversial findings may be at least partially because of the differences in the diseases studied.

Conclusion

Here, we identified *hpo* as a modifier of *dFIG4*, a CMT4J-causing gene. This discovery will contribute

toward clarifying the pathogenesis of CMT as well as the development of disease-modifying therapy.

Acknowledgements

The authors acknowledge our lab members for their technical assistance and discussions.

The authors thank all members of the Chromosome engineering laboratory for their helpful discussions, technical support, and suggestions. We thank the Bloomington *Drosophila* stock center, the Vienna *Drosophila* RNAi center, and the Kyoto *Drosophila* Genetic Resource Center for providing us with fly lines.

This study was supported by the Japan Agency for Medical Research and Development (AMED) (17dk0207030h0002 and 17ek0109222h0001; to T.T.) and JSPS KAKENHI Grant Numbers JP26893227 and JP16K19519; by a Grant for Joint Research Project of The Center for Advanced Insect Research Promotion, Kyoto Institute of Technology; and by a Grant-in-Aid by the Nakabayashi Trust for ALS Research, Tokyo, Japan (Y.A.) and by a Grant for the JSPS Core-to-Core Program, Asia-Africa Science Platforms, and the JSPS Program for Advancing Strategic International Networks to Accelerate the Circulation of Talented Researchers (grant no. S2802 to M.Y.).

Conflicts of interest

There are no conflicts of interest.

References

1 Timmerman V, Strickland AV, Züchner S. Genetics of Charcot–Marie–Tooth (CMT) Disease within the Frame of the Human Genome Project Success. *Genes* 2014; **5**:13–32.
2 Chow CY, Zhang Y, Dowling JJ, Jin N, Adamska M, Shiga K, *et al.* Mutation of *FIG4* causes neurodegeneration in the pale tremor mouse and patients with CMT4J. *Nature* 2007; **448**:68–72.
3 Denton D, Xu T, Kumar S. Autophagy as a pro-death pathway. *Immunol Cell Biol* 2015; **93**:35–42.
4 Hu YB, Dammer EB, Ren RJ, Wang G. The endosomal–lysosomal system: from acidification and cargo sorting to neurodegeneration. *Transl Neurodegener* 2015; **4**:18.
5 Bonangelino CJ, Nau JJ, Deux JE, Brinkman M, Wurmser AE, Gary JD, *et al.* Osmotic stress-induced increase of phosphatidylinositol 3,5-bisphosphate requires Vac14p, an activator of the lipid kinase Fab1p. *J Cell Biol* 2002; **156**:1015–1028.
6 Nicot AS, Fares H, Payrastre B, Chisholm AD, Labouesse M, Laporte J. The phosphoinositide kinase PIKfyve/Fab1p regulates terminal lysosome mutation in *Caenorhabditis elegans*. *Mol Biol Cell* 2006; **17**:3062–3074.
7 Ferguson CJ, Lenk GM, Meisler MH. Defective autophagy in neurons and astrocytes from mice deficient in PI(3,5)P_2. *Hum Mol Genet* 2009; **18**:4868–4878.
8 Kyotani A, Azuma Y, Yamamoto I, Yoshida H, Mizuta I, Mizuno T, *et al.* Knockdown of the *Drosophila FIG4* induces deficient locomotive behavior, shortening of motor neuron, axonal targeting aberration, reduction of life span and defects in eye development. *Exp Neurol* 2016; **277**:86–95.
9 Bharadwaj R, Cunningham KM, Zhang K, Lloyd TE. FIG4 regulates lysosome membrane homeostasis independent of phosphatase function. *Hum Mol Genet* 2016; **25**:681–692.
10 Yamaguchi M, Azuma Y, Yoshida H. ALS and cancer. *J Carcinog Mutagen* 2016; **7**:e122.
11 Staley BK, Irvine KD. Hippo signaling in Drosophila: recent advances and insights. *Dev Dyn* 2012; **241**:3–15.
12 Wang SP, Wang LH. Disease implication of hyper-Hippo signaling. *Open Biol* 2016; **6**:160119.
13 Lee JK, Shin JH, Hwang SG, Gwag BJ, McKee AC, Lee J, *et al.* MST1 functions as a key modulator of neurodegeneration in a mouse model of ALS. *Proc Natl Acad Sci USA* 2013; **110**:12066–12071.
14 Zhang M, Tao W, Yuan Z, Liu Y. Mst-1 deficiency promotes post-traumatic spinal motor neuron survival via enhancement of autophagy flux. *J Neurochem* 2017; **143**:244–256.
15 Wilkinson DS, Jariwala JS, Anderson E, Mitra K, Meisenhelder J, Chang JT, *et al.* Phosphorylation of LC3 by the Hippo kinases STK3/STK4 is essential for autophagy. *Mol Cell* 2015; **57**:55–68.
16 Calamita P, Fanto M. Slimming down fat makes neuropathic hippo: The Fat/Hippo tumor suppressor pathway protects adult neurons through regulation of autophagy. *Autophagy* 2011; **7**:907–909.
17 Takahashi Y, Hirose F, Matsukage A, Yamaguchi M. Identification of three conserved regions in the DREF transcription factors from *Drosophila melanogaster* and *Drosophila virilis*. *Nucleic Acids Res* 1999; **27**:510–516.
18 Ly LL, Suyari O, Yoshioka Y, Tue NT, Yoshida H, Yamaguchi M. dNF-YB plays dual roles in cell death and cell differentiation during *Drosophila* eye development. *Gene* 2013; **520**:106–118.
19 Stewart BA, Atwood HL, Renger JJ, Wang J, Wu CF. Improved stability of *Drosophila* larval neuromuscular preparations in haemolymph-like physiological solutions. *J Comp Physiol A* 1994; **175**:179–191.
20 Nichols CD, Becnel J, Pandey UB. Methods to assay *Drosophila* behavior. *J Vis Exp* 2012; **61**:e3795.
21 Sanhueza M, Chai A, Smith C, McCray BA, Simpson TI, Taylor JP, *et al.* Network analyses reveal novel aspects of ALS pathogenesis. *PLoS Genet* 2015; **11**:e1005107.
22 Rudge SA, Anderson DM, Emr SD. Vacuole size control: regulation of PtdIns (3,5)P2 levels by the vacuole-associated Vac14-Fig4 complex, a PtdIns(3,5) P2-specific phosphatase. *Mol Biol Cell* 2004; **15**:24–36.